S.T. Yau High School Science Award

Research Report

The Team

Name of team member: Qian Wei

School: Rye Country Day School

City, Country: Rye, NY 10580 USA

Name of supervising teacher: Meng Zheng

Job Title: Associate Professor

School/Institution: Institute of Oceanology, Chinese Academy of Sciences

City, Country: Qingdao, 266071, China

Title of Research Report

Enhanced Photocatalytic Degradation of Polyethylene Microplastics under Simulated Sunlight Using Fe3O4@TiO2/Ag Nanocomposite and Optimization via Response Surface Methodology

Date

August 24, 2025

Enhanced Photocatalytic Degradation of Polyethylene Microplastics under Simulated Sunlight Using Fe3O4@TiO2/Ag Nanocomposite and Optimization via Response Surface Methodology

Qian Wei

Abstract

Microplastics present serious environmental and health threats, and traditional disposal methods often fall short in efficiency and can cause ecological damage. Photocatalytic degradation has become a promising approach. However, conventional TiO_2-based photocatalysts suffer from high rates of electron-hole recombination, narrow visible light absorption, and poor reusability. In this study, we develop and optimize a Fe_3O_4@TiO_2/Ag nanocomposite for the efficient degradation of polyethylene microplastics with facile recovery. The synergistic integration of Fe_3O_4 and Ag with TiO_2 enhances visible light absorption and mitigates charge carrier recombination. Notably, the Fe_3O_4@TiO_2/Ag nanocomposite exhibits a degradation efficiency of 15.54%, outperforming Fe_3O_4@TiO_2 (12.63%) and pristine TiO_2 (1.15%). Moreover, the composite maintains its performance over five consecutive cycles, underscoring its durability. The degradation efficiency of Fe_3O_4@TiO_2/Ag was further optimized using response surface methodology. Overall, the developed Fe_3O_4@TiO_2/Ag nanocomposite exhibits excellent photocatalytic efficiency, magnetic recoverability, and long-term stability, highlighting its potential for practical applications in mitigating microplastic pollution.

Keywords: Microplastic · TiO_2, Ag nanoparticles, Magnetic separation, Photocatalysis, Response surface methodology

Contents

1 Introduction 1

2 Method 3

2.1 Materials ……..…….……. 3

2.2 Synthesis of Fe_3O_4 nanoparticles ……..…….. 3

2.3 Synthesis of Fe_3O_4@TiO_2 nanocomposites …….…… 3

2.4 Synthesis of Fe_3O_4@TiO_2/Ag nanocomposites ……... 4

2.5 Characterization …… 5

2.6 Photocatalytic degradation experiments …….…… 5

2.6 Electrochemical measurements …… 6

2.7 Experimental design and response surface methodology …….. 6

3 Results and discussions 7

3.1 Characterization of nanocomposites …… 7

3.2 Photocatalytic performance …….. 11

3.3 Investigation of reaction mechanisms …….. 14

3.4 Optimization with response surface methodology …….. 16

4 Conclusion 19

5 Future perspectives 20

6 Acknowledgement 21

7 References 22

8 Commitments on Academic Honesty and Integrity 26

9 Declaration of Academic Integrity 27

Introduction

Plastics have become an essential part of contemporary society because of their affordability, lightweight nature, high strength, and durability[1,2]. However, these advantages come with significant environmental costs. Annually, approximately 400 million tons of plastic waste are produced, of which 9% is recycled, while the remained ends up in landfills or the ocean[3,4]. Over time, this plastic waste eventually decomposes into microplastics—particles smaller than 5 millimeters in size—entering the environment through littering, river runoff, and wastewater discharge[5]. Currently, about 5.25 trillion microplastics particles, weighing 268,940 tons, are present in oceans and are found in 49% of North Atlantic fish[6,7]. Carrying toxic, endocrine-disrupting chemicals, microplastics have already entered human bodies via the food chain, threatening human health at this very moment[8]. Given the scale of microplastic pollution and its associated hazards, there is an urgent need for effective microplastics degradation approaches.

Photocatalytic degradation has surfaced as a promising method for eliminating organic pollutant due to its high efficiency, utilization of renewable light energy, and avoidance of toxic byproducts in contrast to traditional methods such as landfilling and waste incineration[9]. Among various photocatalysts, anatase titanium dioxide (TiO_2) has been extensively studied due to its affordability, chemical stability, and powerful oxidizing properties[10]. When exposed to light irradiation, electrons in TiO_2 are excited from the valence band (VB) to the conduction band (CB), resulting in the formation of positively charged holes (h+) in the VB. These electron-hole pairs react with water and oxygen to generate reactive oxygen species (ROS), including hydroxyl radicals (•OH) and superoxide radicals ($\bullet O_2^-$), which degrade microplastics into lower molecular weight compounds[11]. However, TiO_2 is hindered by a high rate of electron-hole recombination and limited absorption of visible light because of its large band gap (3.2 eV)[12].

To overcome these limitations, several methods have been investigated to enhance the mobility of charge carriers, such as metallic modification and heterojunction engineering[13]. Of the various metals examined, silver (Ag) has attracted considerable interest because of its plasmonic properties. Ag nanoparticles can enhance light absorption and facilitate electron excitation via the surface plasmon resonance (SPR) effect[14]. Previous studies have shown that depositing Ag nanoparticles onto TiO_2 can reduced its band gap from 3.2 eV to approximately 2.75 eV, thereby enabling photocatalytic activity under visible light[15]. Ag/TiO_2 photocatalysts have demonstrated significant performance enhancements, achieving degradation efficiencies of 99.3% for methyl orange in 80 min and 98% for Congo red in 4 h[16,17]. Despite these improvements, Ag/TiO_2 composite often suffers from poor reusability, limiting practical application.

Incorporating magnetic materials, such as iron oxide (Fe_3O_4) offers an effective solution for catalyst recovery via magnetic separation. Embedding Fe_3O_4 into TiO_2 not only enhances recoverability but also can enhance photocatalytic activity. For instance, Fe_3O_4/TiO_2 hollow spheres exhibited superparamagnetic characteristics at room temperature and maintain good photocatalytic activity under UV light irradiation, with minimal efficiency loss after up to six recovery cycles[18]. Additionally, the formation of a p-n heterojunction at the Fe_3O_4/TiO_2 interface creates an interfacial electric field that promotes charge carrier mobility, further improving photocatalytic efficiency[19].

These findings underscore the potential of integrating Ag and Fe_3O_4 into TiO_2 to simultaneously enhance photocatalytic performance and reusability. However, the synergistic effects of Ag and Fe_3O_4 on the degradation of polyethylene (PE) microplastics remain relatively underexplored. This study aims to develop and optimize a highly efficient, magnetically recoverable, and stable Fe_3O_4@TiO_2/Ag photocatalyst. By strategically incorporating p-n heterojunctions, the Schottky barrier, and the SPR effect, this proposed design seeks to

maximize photocatalytic efficiency, offering a promising approach for the degradation of microplastics in real-world environmental applications.

Methodology

Materials

Ammonia solution ($NH_3 \cdot H_2O$), tetrabutyl titanate (TBOT, $C_{16}H_{36}O_4Ti$), and isopropanol (C_3H_8O) were purchased from Aladdin Co., Ltd. (China). Iron (III) chloride hexahydrate ($FeCl_3 \cdot 6H_2O$), iron (II) chloride tetrahydrate ($FeCl_2 \cdot 4H_2O$), silver nitrate ($AgNO_3$), p-benzoquinone (p-BQ), methanol (MeOH), and tert-butanol (TBA) were obtained from Sinopharm Group Chemical Reagent Beijing Co., Ltd. (China). Deionized water with a resistivity greater than 18.2 MΩ cm was obtained using a Millipore Milli-Q Plus 185 purification system and was used in all experiments. All reagents were used as received, without further purification.

Synthesis of Fe_3O_4 nanoparticles

Fe_3O_4 nanoparticles were synthesized through a co-precipitation method[20]. In a standard procedure, 2.36 g of $FeCl_3 \cdot 6H_2O$ and 2.5 g of $FeCl_2 \cdot 4H_2O$ were dissolved in 100 mL of deionized (DI) water and stirred for 30 min. Following this, $NH_3 \cdot H_2O$ was added dropwise until a black precipitate appeared. The precipitate was subsequently collected using a magnet, washed three times with ethanol and DI water, and dried under vacuum at 50 °C for 6 hours.

Synthesis of Fe_3O_4@TiO_2 nanocomposites

Fe_3O_4@TiO_2 nanocomposites were prepared by a hydrothermal method. A specified quantity of Fe_3O_4 (as listed in Table 1) was dispersed in 100 mL of isopropanol that contained 426 mg of TBOT through sonication for 30 min. Next, 20 mL of DI water was added, and the resulting mixture was placed in a 50 mL Teflon-lined autoclave and allowed to react at 180 ℃ for 12 hours. Once the mixture cooled to room temperature, the precipitate was separated using

a magnet and then washed three times with ethanol and deionized water. It was then dried at 50°C for six hours.

Synthesis of Fe_3O_4@TiO_2/Ag nanocomposites

Fe_3O_4@TiO_2/Ag nanocomposites were synthesized via sonicating varying volumes of $AgNO_3$ solution (Table 1) with the Fe_3O_4@TiO_2 nanocomposite. Specifically, Fe_3O_4@TiO_2 was suspended in 50 mL of deionized water and 10 mL of ethanol, and then subjected to sonication for 2 hours. The resulting product was then filtered, thoroughly washed, and dried at 50°C for 6 h. A schematic illustration of the synthesis process is presented in Fig. 1.

Table 1 Composition details for the synthesis of Fe_3O_4@TiO_2/Ag nanocomposites with varying Fe_3O_4 and Ag ratios.

Ratio	TiO_2 (mg)	Fe_3O_4 (mg)	Ag (mg)	0.005 M $AgNO_3$ (mL)
60% Fe_3O_4 + 5% Ag	100	60	5	9.3
70% Fe_3O_4 + 3% Ag	100	70	3	5.6
70% Fe_3O_4 + 7% Ag	100	70	7	13.0
100% Fe_3O_4 + 2% Ag	100	100	2	3.7
100% Fe_3O_4 + 5% Ag	100	100	5	9.3
100% Fe_3O_4 + 8% Ag	100	100	8	14.8
130% Fe_3O_4 + 3% Ag	100	130	3	5.6
130% Fe_3O_4 + 7% Ag	100	130	7	13.0
140% Fe_3O_4 + 5% Ag	100	140	5	9.3

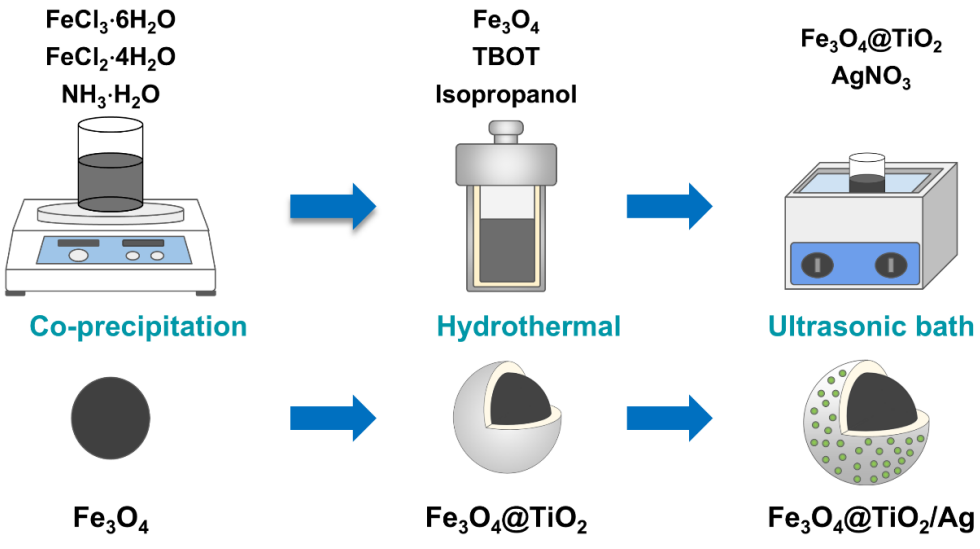

Fig. 1. Schematic representation of the synthesis process for Fe_3O_4@TiO_2/Ag.

Characterization

The morphology of the prepared samples was observed using scanning electron microscopy (SEM, S-4800, Japan). The crystal structure was characterized by X-ray diffraction (XRD) using a Bruker D8 Advance diffractometer (German) with Cu Kα radiation. The optical properties were examined through UV-Vis diffuse reflectance spectroscopy (DRS, HITACHI U-3900H, Japan) and photoluminescence spectroscopy (PL, Hitachi F7000, Japan) with excitation at 325 nm. Images of the polyethylene are taken using a digital microscope (ZY-HDMI200M, China) and analyzed using ImageJ software for observe particle size distribution. The chemical composition of the degraded polyethylene was analyzed using Fourier transform infrared spectroscopy (FTIR, Thermo Scientific Nicolet iS50, USA).

Photocatalytic degradation experiments

The effectiveness of the synthesized materials in photocatalysis was assessed by evaluating their performance in the degradation of PE microplastics within a custom-designed photoreactor. The system employed a 300 W xenon lamp (full spectrum) to simulate sunlight conditions and a mechanical stirrer to ensure uniform dispersion of both the photocatalyst and the PE microplastics in the solution. In each experiment, 50 mg of the photocatalyst and 10 mg of PE microplastics were dispersed in 100 mL of DI water, followed by continuous stirring and light irradiation for 3 h. After the reaction, the photocatalysts were separated from the mixture: Fe_3O_4@TiO_2 and Fe_3O_4@TiO_2/Ag were magnetically retrieved, while non-magnetic TiO_2 is separated using centrifugation. The remaining suspension was then vacuum-filtered, and the collected PE particles underwent further analysis. The degradation efficiency (η) was determined using the following equation:

$$\eta = \left(1 - \frac{A_f}{A_i}\right) \times 100\% \quad (1)$$

where A_i represents the initial average area, and A_f represents the final average area of the PE microplastics particles.

To investigate the main active oxygen species, quenching experiments are tested by adding 10 mM of p-BQ, MeOH, and TBA to evaluate the contributions of $\bullet O_2^-$, •OH, and h^+ in the degradation process.

Electrochemical measurements

Electrochemical measurements were performed on CHI760 electrochemical workstation (CH Instruments, China) with a standard three-electrode system with as-prepared sample, Pt electrode, and SCE electrode as working electrode, counter electrode, and reference electrode, respectively. The preparation method of working electrode was as follows: 2 mg samples, 995 μL ethanol and 5 μL Nafion are ultrasonically mixed for 30 min to prepare slurry. Then the slurry of 50 μL was dropped on the indium tin oxide (ITO) glass, and dried at room temperature. Using 0.5 M of sodium sulfate (Na_2SO_4) solution as electrolyte. Electrochemical impedance spectroscopy (EIS) was performed under 10^5 Hz to 10^{-2} Hz with 5 mV amplitude under the open-circuit potential (OCP).

Experimental design and response surface methodology

The composition of the photocatalyst was optimized using Response Surface Methodology (RSM) to identify the optimal conditions for maximum photocatalytic degradation efficiency. A Central Composite Design (CCD) was employed to evaluate both the linear and quadratic effects of two key independent variables, Fe_3O_4 (A, wt%) and Ag (B, wt%), on PE microplastic degradation. Each variable was assessed at five different levels ($-\alpha$, -1, 0, $+1$, $+\alpha$). The experimental design was conducted using the Design Expert software, with Fe_3O_4 levels ranging from 60 to 140 wt% and Ag levels ranging from 2 to 8 wt%, as summarized in Table 2.

Table 2 Experimental ranges and levels of independent variables for polyethylene degradation. α = 1.414 (axial point for CCD for two factors), with the actual values rounded

Independent variable	Range and level				
weight percentage	−α	−1	0	+1	+α
Fe_3O_4 (A, wt%)	60	70	100	130	140
Ag (B, wt%)	2	3	5	7	8

Results and discussion

Characterization of nanocomposites

The morphology of the composites was characterized using scanning electron microscopy (SEM). As shown in Fig. 2, the samples exhibit predominantly monodispersed, quasi-spherical particles that tend to aggregate, likely due to magnetic interactions and surface energy minimization[21]. The average particle sizes increase from 18.58 nm for Fe_3O_4 nanoparticles to 23.24 nm after TiO_2 coating, and further to 24.50 nm following Ag deposition. These progressive size increments confirm the successful formation of the TiO_2 shell and subsequent Ag deposition on the Fe_3O_4 core.

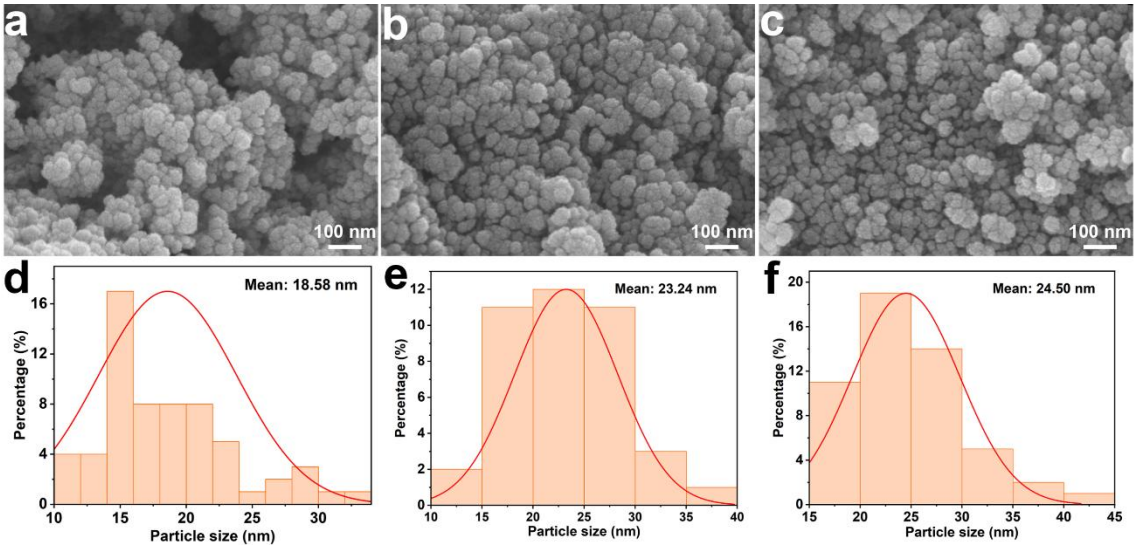

Fig. 2. SEM images and particle size distributions of Fe_3O_4 (a, d), Fe_3O_4@TiO_2 (b, e), and Fe_3O_4@TiO_2/Ag (c, f).

The X-ray diffraction (XRD) patterns of Fe_3O_4, Fe_3O_4@TiO_2, and Fe_3O_4@TiO_2/Ag are shown in Fig. 3, revealing distinct diffraction peaks that confirm the high crystallinity of the composites. In the Fe_3O_4 sample, characteristic peaks at 2θ values of 30.2°, 35.6°, 37.2°, 43.2°, 47.3°, 53.6°, 57.2°, and 62.8°can be indexed to the (220), (311), (222), (400), (422), (511), and (440) crystal planes of the cubic magnetite phase (PDF#97-015-8743). The XRD pattern for the Fe_3O_4@TiO_2 composite displays additional diffraction peaks at 2θ values of 25.2°, 37.8°, 47.9°, 53.8°, 55.0°, and 62.5°, which correspond to the (101), (004), (200), (105), (211), and (204) planes of the tetragonal anatase phase of TiO_2 (PDF#99-000-0105). These anatase-specific peaks confirm the successful coating of the TiO_2 shell on the Fe_3O_4 core[22]. Furthermore, the XRD patterns of the Fe_3O_4@TiO_2/Ag composite reveals two additional diffraction peaks at 2θ values of 38.1° and 64.4°. These peaks are attributed to the (111) and (220) planes of the cubic phase of Ag (PDF#97-060-4632), thereby verifying the successful deposition of Ag onto the Fe_3O_4@TiO_2 core/shell nanocomposite[23].

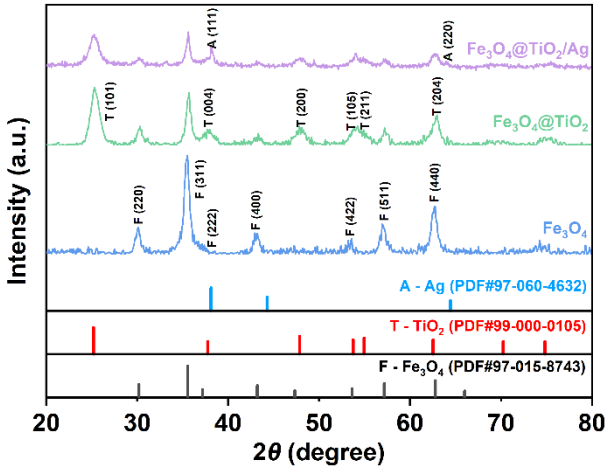

Fig. 3. XRD patterns of Fe_3O_4, Fe_3O_4@TiO_2, and Fe_3O_4@TiO_2/Ag samples.

The optical properties of the synthesized photocatalysts were examined by UV-vis DRS. As shown in Fig. 4a, pure TiO_2 exhibits strong absorption edge below 400 nm, corresponding to the UV light range. In comparison, Fe_3O_4@TiO_2 shows an enhanced absorption in visible light region, while the Fe_3O_4@TiO_2/Ag shows even higher absorption across the entire visible

spectrum. The band gap (E_g) of the photocatalyst was estimated using Tauc plots based on the Kubelka-Munk function, as described by the equation:

$$\alpha h\nu = A\ (h\nu - E_g)^{1/n} \quad (2)$$

where α, h, A, and E_g represent the absorption coefficient, Planck's constant, the frequency of incident light, a constant, and the band gap energy, respectively[24]. For anatase TiO_2, the value of n is set to 2, reflecting its indirect band gap nature. The E_g was determined by extrapolating the linear segment of the Tauc plot to the y-axis intercept at zero. As shown in Fig. 4b, the estimated E_g for TiO_2, Fe_3O_4@TiO_2 and Fe_3O_4@TiO_2/Ag is 3.29 eV, 3.05 eV, and 2.40 eV, respectively. Notably, under light irradiation, when the free electrons on the Ag surface oscillate collectively at the same frequency as the incident light, a phenomenon referred to as surface plasmon resonance, an intense localized electric field is generated. This field facilitates the generation and separation of charge carriers, thereby lowering the energy needed for electron excitation from the VB to CB. Additionally, SPR-induced photon scattering increases the optical path length of incident photons, further improving light utilization[25]. These results indicate that the incorporation of Fe_3O_4 and Ag not only narrows the band gap of TiO_2 but also extends its light absorption capabilities into the lower energy region.

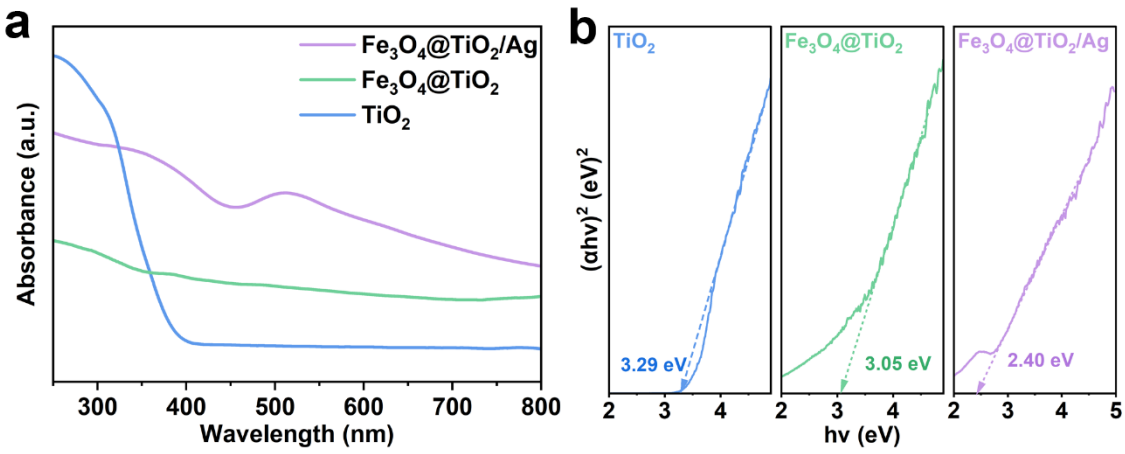

Fig. 4. (a) UV-vis DRS and (b) Tauc plots of Fe_3O_4, Fe_3O_4@TiO_2, and Fe_3O_4@TiO_2/Ag samples.

Photoluminescence (PL) spectroscopy captures light emitted by a material as electrons fall from the excited state to the ground state upon irradiation by a laser beam. PL spectra provide valuable insight into the electron-hole recombination dynamics of a material because, as recombination happens, the input energy is dissipated as emitted light[26]. Therefore, a high PL intensity indicates a high electron-hole recombination rate. As shown in Fig. 5, pure TiO_2 exhibits the highest PL intensity, with a strong peak around 400 nm and 500 nm, suggesting a rapid electron-hole recombination process. Upon incorporation of Fe_3O_4 into TiO_2, an observable drop in the PL intensity is observed, which can be ascribed to the formation of a p-n heterojunction: TiO_2, an n-type semiconductor rich in electrons, is interfaced with Fe_3O_4, a p-type semiconductor with an abundance of holes. At their interface, electrons diffuse from the conduction band of TiO_2 into that of Fe_3O_4, while holes move in the opposite direction, thereby forming an internal electric field that effectively facilitates charge separation and prolongs the lifetimes of the charge carrier[27]. Furthermore, the Fe_3O_4@TiO_2/Ag nanocomposite exhibits the lowest PL intensity among the samples, indicating the most effective suppression of electron-hole recombination. This improvement can be attributed to the Schottky barrier created at the Ag-TiO2 interface. As metal and semiconductor, Ag and TiO2, respectively, have different Fermi levels. To achieve thermodynamic equilibrium, electrons flow from TiO2 (higher Fermi level) to Ag (lower Fermi level). This electron movement aligns their Fermi levels and creates a layer of positive charges embedded in the TiO2's crystal lattice, which generate an electric field directed from the TiO2 to the Ag, thus creating a potential barrier that impede low-energy electrons from returning to the TiO2, effectively separating the electrons and holes[25].

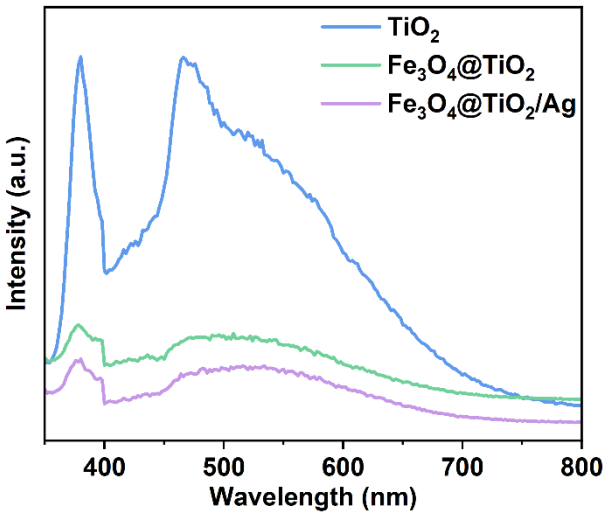

Fig. 5. PL spectra of obtained samples.

Photocatalytic performance

The photocatalytic degradation efficiency of PE microplastics was tested under simulated solar irradiation. As shown in Fig. 6a, pure TiO_2 showed only a 1.152% degradation rate, suggesting limited photocatalytic activity, likely due to poor light absorption and electron-hole recombination. In contrast, the Fe_3O_4@TiO_2 demonstrated a notable improvement, with a degradation rate of 12.63%, indicating enhanced photocatalytic efficiency, potentially due to improved charge separation at the p-n heterojunction interface. The highest degradation rate was observed with the Fe_3O_4@TiO_2/Ag, achieving a 15.54% degradation rate. Incorporating Ag nanoparticles likely further improved electron-hole separation through the Schottky barrier and extended light absorption to the visible spectrum by SPR, improving the photocatalytic activity. While this 15.54% degradation efficiency appears low compared to reported values for other organic pollutants like dyes (>90%), this discrepancy primarily reflects the inherent recalcitrance of polyethylene (PE) microplastics rather than a lack of photocatalytic performance. PE consists of a long chain of ethylene with strong, nonpolar C-C and C-H bonds and no functional groups, making it chemically inert and highly hydrophobic. These characteristics hinder interaction with ROS and limit surface adsorption, hence impeding photocatalytic degradation. In contrast, dyes such as methylene blue and Congo red often

contain aromatic rings that are more susceptible to ROS attack. Congo red additionally contains azo bonds (-N=N-) that serve as reactive sites for ROS. Moreover, dyes have chromophores that absorb light directly and tend to adsorb readily onto catalyst surfaces via electrostatic or π–π interactions, facilitating degradation[28].

Despite PE's resistance to photocatalytic breakdown, our degradation efficiency is comparable to, or exceeds, previously reported values for polyethylene and similar polymers under similar conditions, as summarized in Table 3. Our catalyst achieved superior degradation efficiency within a shorter timeframe compared to most studies targeting microplastics, including those focused specifically on PE.

It is also critical to assess the reusability of photocatalysts as this is an important factor to consider for real-world applications. In Fig. 6b, a minimum reduction in degradation rate is observed over five consecutive trails, suggesting that the Fe_3O_4@TiO_2/Ag nanocomposite can maintain its structure integrity and catalytic activity over repeated use. The high stability demonstrates that Fe_3O_4@TiO_2/Ag could serve as an economical and sustainable photocatalyst for long-term plastic degradation in water.

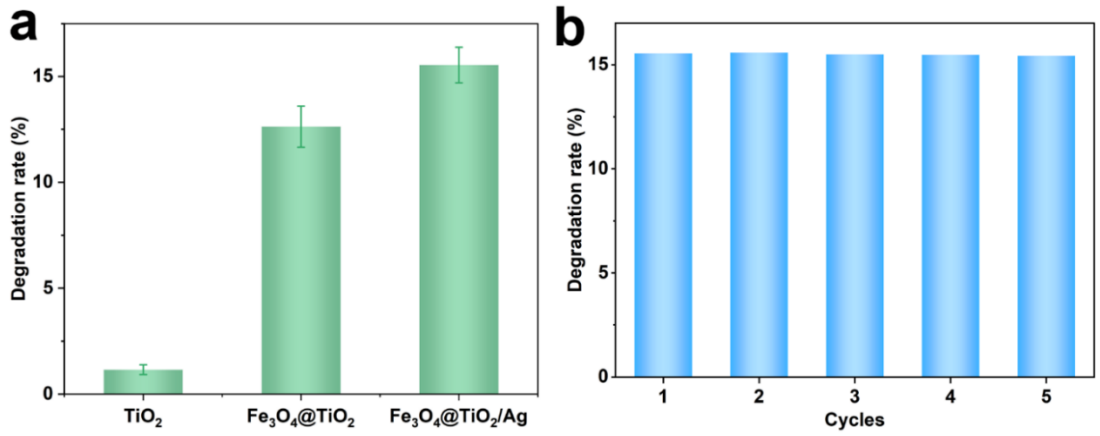

Fig. 6. (a) PE microplastics degradation efficiency with TiO_2, Fe_3O_4@TiO_2, and Fe_3O_4@TiO_2/Ag. Error bars are standard error values of three tests (n = 2); (b) Degradation efficiency of Fe_3O_4@TiO_2/Ag photocatalyst for PE microplastics degradation over five recycling

Table 3. Overview of photocatalytic MP degradation.

Photocatalyst	MP type	Light source	Degradation efficiency/time	Ref
ZnO NRs	PP	visible	65% / two weeks	[29]
TiO2	PP	visible	50.5% / 50h	[30]
N-TiO2	PE	visible	4.65% / 50h	[31]
TiO_x/ZnO	PE	UV	50% / 168h	[32]
Ag_2O/Fe-MOF	PE	UV-Vis	15.8% / 8h	[33]
$Bi_4Ti_3O_{12}$	PE	UV-Vis-IR	38.27% / 6h	[34]
α-Fe_2O_3/*g*-C_3N_4	PS	visible	7.81% / 30 days	[35]
BiOI-Fe_3O_4	PS	visible	64% / 120h	[36]
ZIF-67/g-C_3N_4	PET	UV-Vis	60.63% / 6h	[37]
Bi2O3@N-TiO2	PET	UV-Vis-IR	10.23% / 48h	[38]
This study	**PE**	**UV-Vis-IR**	**15.54% / 3h**	

The surface chemical changes in PE microplastics after degradation were analyzed by FTIR spectra. Fig. 7 compares the FTIR spectra of PE before and after photocatalytic degradation. The photodegraded PE microplastics exhibit a noticeable decrease in the intensity of characteristic peaks, suggesting that the PE polymer chains have been broken into shorter fragments. A new peak at 1710 cm^{-1} appeared after degradation, corresponding to the carbonyl (C=O) stretching vibrations, suggesting the formation of carbonyl compounds such as ketones, aldehydes, and carboxylic acids[39], which are key degradation products formed during oxidative degradation of microplastics.

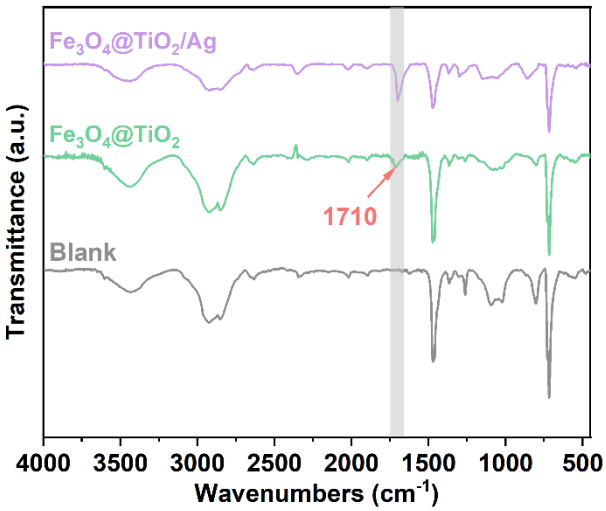

Fig. 7. FTIR spectra of PE, PE degraded with Fe_3O_4@TiO_2 and Fe_3O_4@TiO_2/Ag.

Investigation of reaction mechanisms

To evaluate the efficiency of charge carrier separation in the catalysts, transient photocurrent measurements and were conducted. As shown in Fig. 8a, all samples exhibited stable and repeatable photocurrent responses under periodic visible-light illumination, indicating effective and sustained charge separation. In Fe_3O_4@TiO_2, the formation of heterojunctions facilitates the spatial separation of electrons and holes, resulting in an increased photocurrent response, which is 3.1 times higher than that of pure TiO_2. Among the tested samples, the Fe_3O_4@TiO_2/Ag exhibited the highest photocurrent density of 3.654 $\mu A \cdot cm^{-2}$, which is 4.6 and 1.5 times higher than that of Fe_3O_4@TiO_2 and TiO_2. Similarly, in the EIS Nyquist plots, the Fe_3O_4@TiO_2/Ag exhibits the smallest semicircle diameter, indicating the lowest charge transfer resistance and suggesting more efficient separation of photogenerated charge carriers. Effective separation of electron–hole pairs is crucial for enhancing photocatalytic performance[40]. Moreover, the formation of heterojunctions and the incorporation of Ag nanoparticles significantly improve the charge transport kinetics of Fe_3O_4@TiO_2/Ag, effectively suppressing electron–hole recombination and

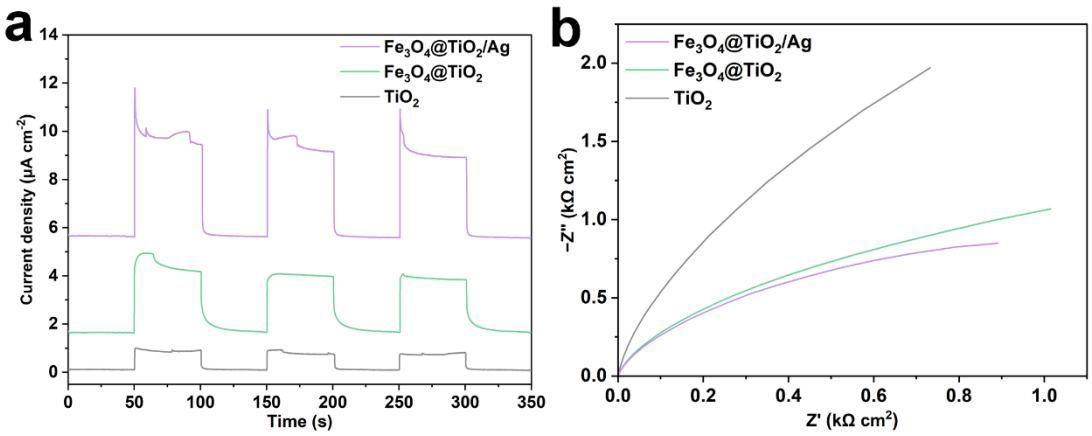

Fig. 8. (a) Transient photocurrent responses of TiO_2, Fe_3O_4@TiO_2, and Fe_3O_4@TiO_2/Ag. (b) The EIS Nyquist plots of TiO_2, Fe_3O_4@TiO_2, and Fe_3O_4@TiO_2/Ag.

To elucidate the catalytic degradation mechanism of PE microplastics by the Fe_3O_4@TiO_2/Ag, specific scavengers were employed to identify the reactive species involved: p-BQ for $\bullet O_2^-$, MeOH for h^+, and TBA for •OH[41]. These scavengers enabled the identification of the predominant reactive species involved in the photocatalytic process. As shown in Fig. 9, the addition of each scavenger significantly suppressed the degradation efficiency of PE microplastics compared to the control, indicating that $\bullet O_2^-$, h^+, and •OH are the primary reactive species responsible for the photocatalytic decomposition of PE microplastics by the composite.

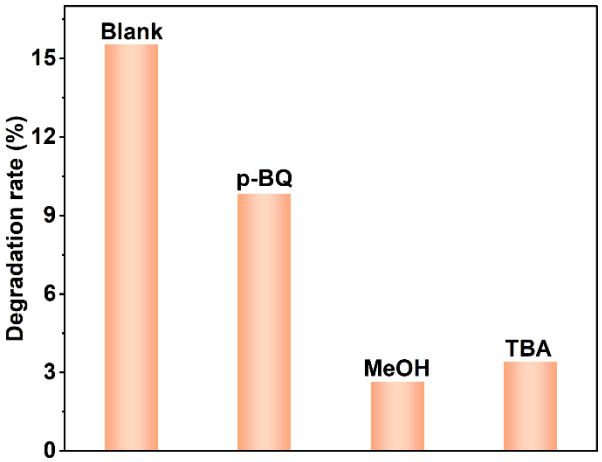

Fig. 9. (a) Transient photocurrent responses of Fe_3O_4@TiO_2/Ag.

Fig. 10 illustrates the photocatalytic degradation mechanism of PE microplastics by the catalyst. Under visible light irradiation, TiO_2, Fe_3O_4, and Ag are photoactivated to initiate the

degradation process. Upon excitation, electrons transition from the valence band (VB) to the conduction band (CB) in TiO_2 and Fe_3O_4, creating holes in the valence band. These photogenerated holes can directly oxidize PE microplastics in water. Additionally, the holes can oxidize water molecules to generate hydroxyl radicals (•OH), which further contribute to the degradation of PE through strong oxidative activity. Meanwhile, the electrons in the CB reduce dissolved oxygen to superoxide radicals ($•O_2^-$), which also participate in the oxidative degradation of PE microplastics.

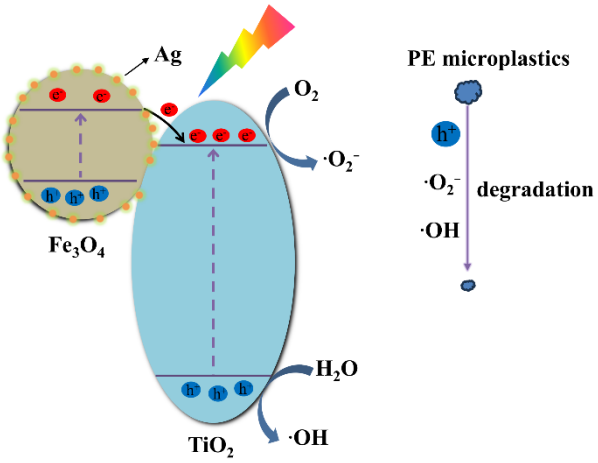

Fig. 10. Mechanism of photocatalytic degradation PE microplastics over Fe_3O_4@TiO_2/Ag.

Optimization with response surface methodology

Response surface methodology (RSM) was employed to optimize the photocatalytic performance. A two-factor, five-level Central Composite Design (CCD) was used, with thirteen experiments conducted, yielding a quadratic model with high statistical significance ($p < 0.0001$) (Table 4). Based on the experimental design and obtained responses, linear, two-factor interaction (2FI), quadratic, and cubic models are fitted and evaluated, whose summary is shown in Table 5. The quadratic model is identified as the most suitable and representative of the data, as suggested by the highly significant p-value ($p < 0.0001$) and strong correlation, R^2,

between the model and the experimental data. The relationship can be mathematically represented as follows:

$$\eta = 15.84254 + 0.223831A + 6.63873B - 0.003188AB - 0.000573A^2 - 0.675653B^2 \quad (3)$$

where η, A, and B represents the degradation efficiency, Fe_3O_4 wt%, and Ag wt%. This equation, expressed in terms of actual factors, can be utilized to forecast the response based on specific levels of each factor, thereby identifying the optimal outcome.

Table 4 Two factors five levels CCD design and experimental result

Run	Fe_3O_4 wt%	Ag wt%	Degradation %
1	−1	−1	9.893
2	1	−1	16.93
3	−1	1	8.179
4	1	1	14.463
5	−α	0	11.242
6	+α	0	17.682
7	0	−α	11.052
8	0	+α	9.126
9	0	0	15.411
10	0	0	15.809
11	0	0	14.823
12	0	0	15.913
13	0	0	15.742

Table 5 Fit summary of models

Model	Sequential p-value	Lack of Fit p-value	Adjusted R^2	Predicted R^2	
Linear	0.0168	0.0012	0.4702	0.1965	
2FI	0.8815	0.0009	0.4128	0.009	
Quadratic	**< 0.0001**	**0.0977**	**0.9543**	**0.8458**	**Suggested**
Cubic	0.0292	0.7862	0.9844	0.9815	Aliased

In Table 6, the ANOVA results reveal that the overall model is statistically significant (p-value < 0.0001), meaning it effectively models the variability in the response. Among the factors, Fe_3O_4 has the strongest influence, supported by its high F-value (134.03) and low p-value ($p < 0.0001$), showing that changes in Fe_3O_4 concentration have a substantial impact on the degradation. Ag is also a significant factor (p-value = 0.0092), though its effect is smaller than Fe_3O_4. The quadratic term for Ag (B^2) is highly significant ($p < 0.0001$), indicating a nonlinear relationship between Ag concentration and the degradation rate. In contrast, the quadratic term for Fe_3O_4 (A^2) is not significant (p-value = 0.0872), suggesting its effect is primarily linear. The interaction between Fe_3O_4 and Ag (AB) is insignificant (p-value = 0.5996), meaning these factors influence the response independently. Additionally, the model fits the data well, as the lack of fit is insignificant (p-value = 0.0977).

Table 6 Analysis for variance (ANOVA) results of fitted model

Source	Sum of Squares	df	Mean Square	F-value	p-value	
Model	119.98	5	34	51.15	**< 0.0001**	significant
A-Fe_3O_4	62.88	1	62.88	134.03	< 0.0001	
B-Ag	5.96	1	5.96	12.70	0.0092	
AB	0.1418	1	0.1418	0.3021	0.5996	
A^2	1.85	1	1.853	3.95	0.0872	
B^2	50.81	1	50.81	108.3	< 0.0001	
Residual	3.28	7	0.4692			
Lack of Fit	2.50	3	0.8337	4.26	0.0977	not significant
Pure Error	0.7830	4	0.1958			
Cor Total	123.27	12				

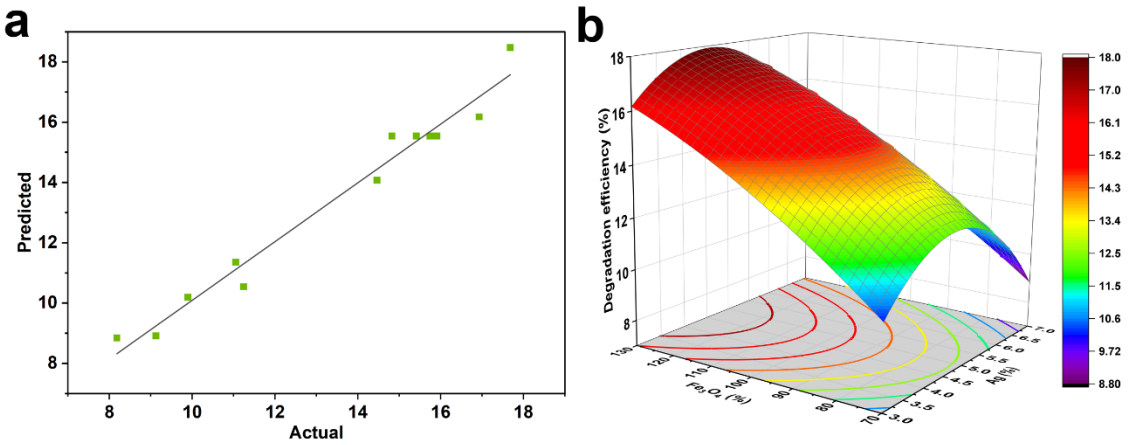

Fig. 11. (a) Curve of actual vs. predicted values and (b) 3D response surface plot.

Fig. 11a compares the actual and predicted values of the degradation rate by the model. The actual values are generally clustered close to the diagonal line (y = x), suggesting that the model predictions are reasonably close to the actual value. Fig. 11b shows the interaction between Fe_3O_4 wt% and Ag wt%. When Ag wt% increased, the degradation rate initially increases and then decreases. This behaviour could be a result of excessive Ag loading that promotes electron-hole recombination, blocks active sites, and hinders charge carriers migration[42]. In comparison, the degradation rate consistently increases as Fe_3O_4 wt% increases, which is consistent with the ANOVA result. The magnitude of change in the response surface is larger on the Fe_3O_4 side than on the Ag side, suggesting that Fe_3O_4 has a greater influence on the degradation rate. The optimal Fe_3O_4 and Ag weight percentages, calculated from the regression model in Eq. 3 are 130% and 4.623%, respectively, with a predicted maximum degradation rate of 17.941%.

Conclusion

In this study, we developed and optimized the Fe_3O_4@TiO_2/Ag photocatalyst for effective polyethylene microplastic degradation. The results suggested that Fe_3O_4 and Ag effectively enhanced the photocatalytic activity of TiO_2 by reducing band gap energy, promoting charge carrier separation, and increasing the light absorption into the visible light range, which could be attributed to the p-n heterojunction at the Fe_3O_4@TiO_2 interface, Schottky barrier at the

TiO_2/Ag interface, and surface plasmon resonance effect of Ag nanoparticles. Under 3 h of simulated solar irradiation, Fe_3O_4@TiO_2/Ag achieved an excellent 15.54% degradation of polyethylene microplastics. Its magnetic properties also allowed easy separation after each degradation, and the nanocomposite showed minimal reduction in efficiency after five reuses. In addition, the weight percentages of Fe_3O_4 and Ag were optimized using response surface methodology (RSM) to maximize the degradation efficiency to 17.941%. In short, the Fe_3O_4@TiO_2/Ag nanocomposite demonstrated great potential in industrial photocatalytic applications in microplastic degradation.

Future perspectives

Despite rapid advancements in the photocatalytic degradation of microplastics, there remain several research gaps that require further attention. Future work in catalyst design should focus on enhancing light absorption, reducing band gap energy, and facilitating efficient charge carrier separation to maximize photocatalytic efficiency. Cost-effectiveness, stability, and retrievability must also be taken into account to guarantee the scalability and practicality of these catalysts for industrial applications. Theoretical modeling and calculation like density functional theory (DFT) and machine learning models can be used to help predict properties and select the desired catalyst. It is also essential to understand the fundamental mechanisms of photocatalytic degradation at the subatomic level, as it can offer valuable insights for rational design of more effective catalysts. Furthermore, future research should focus on understanding the microplastics degradation pathways, identify intermediate byproducts, and evaluate their ecological implications for safety and sustainability considerations. Researching how the degradation products can be recycled to produce value-added fuels, chemicals, and materials is another promising area of study.

Acknowledgement

I wish to express my sincere gratitude to Dr. Meng Zheng for his invaluable guidance and for providing me the opportunity to carry out this independent research in his laboratory at the Institute of Oceanology, Chinese Academy of Sciences. I would also like to thank graduate student Wenhui Ji for her patient instruction on laboratory equipment usage, answering my numerous questions throughout the research process, and providing helpful feedback on this manuscript.

References

[1] Barboza L G A, Lopes C, Oliveira P, et al., Microplastics in wild fish from North East Atlantic Ocean and its potential for causing neurotoxic effects, lipid oxidative damage, and human health risks associated with ingestion exposure, *Sci. Total Environ.* **2020**, *717, 134625.*

[2] Ouyang Z Z, Li S X, Zhao M Y, et al., The aging behavior of polyvinyl chloride microplastics promoted by UV-activated persulfate process, *J. Hazard. Mater.* **2022**, *424, 127461.*

[3] Ermis H, Collins C, Kumar Saha S, et al., Beyond Visibility: Microorganisms for tackling plastic and microplastic problems for cleaner future, *Chemical Engineering Journal* **2024**, *497, 154585.*

[4] Singh N, Walker T R, Plastic recycling: A panacea or environmental pollution problem, *npj Materials Sustainability* **2024**, *2, 17.*

[5] Li Y, Sun Y X, Li J Z, et al., Research on the Influence of Microplastics on Marine Life, *IOP Conference Series: Earth and Environmental Science* **2021**, *631, 012006.*

[6] Eriksen M, Lebreton L C M, Carson H S, et al., Plastic Pollution in the World's Oceans: More than 5 Trillion Plastic Pieces Weighing over 250,000 Tons Afloat at Sea, *PLOS ONE* **2014**, *9, e111913.*

[7] Hansen J, Hildebrandt L, Zimmermann T, et al., Quantification and characterization of microplastics in surface water samples from the Northeast Atlantic Ocean using laser direct infrared imaging, *Marine Pollution Bulletin* **2023**, *190, 114880.*

[8] Goswami S, Adhikary S, Bhattacharya S, et al., The alarming link between environmental microplastics and health hazards with special emphasis on cancer, *Life Sciences* **2024**, *355, 122937.*

[9] Wang C L, Liu N Z, Liu X J, et al., Sulfur vacancy-enhanced In_2S_{3-x} hollow microtubes for photocatalytic Cr (VI) and tetracycline removal, *J. Environ. Manage.* **2024**, *353, 120173.*

[10] Hou C, Wang L, Zhang W, et al., Construction of TiO_{2-x} Confined by Layered Iron Silicate toward Efficient Visible-Light-Driven Photocatalysis-Fenton Synergistic Removal of Organic Pollutants, *ACS Appl. Mater. Interfaces* **2023**, *15, 23124-23135.*

[11] Ge J H, Zhang Z P, Ouyang Z Z, et al., Photocatalytic degradation of (micro)plastics using TiO_2-based and other catalysts: Properties, influencing factor, and mechanism, *Environ. Res.* **2022**, *209, 112729.*

[12] Guo Q, Zhou C Y, Ma Z, et al., Fundamentals of TiO_2 Photocatalysis: Concepts, Mechanisms, and Challenges, *Adv. Mater.* **2019**, *31, 1901997.*

[13] Dong H R, Zeng G M, Tang L, et al., An overview on limitations of TiO_2-based particles for photocatalytic degradation of organic pollutants and the corresponding countermeasures, *Water Res.* **2015**, *79, 128-146.*

[14] Hou W, Cronin S B, A Review of Surface Plasmon Resonance-Enhanced Photocatalysis, *Adv. Funct. Mater.* **2013**, *23, 1612-1619.*

[15] Tunc I, Bruns M, Gliemann H, et al., Bandgap determination and charge separation in Ag@TiO_2 core shell nanoparticle films, *Surf. Interface Anal.* **2010**, *42, 835-841.*

[16] Saravanan R, Manoj D, Qin J, et al., Mechanothermal synthesis of Ag/TiO_2 for photocatalytic methyl orange degradation and hydrogen production, *Process Safety and Environmental Protection* **2018**, *120, 339-347.*

[17] Sowmya S R, Madhu G M, Hashir M, Studies on Nano-Engineered TiO_2 Photo Catalyst for Effective Degradation of Dye, *IOP Conference Series: Materials Science and Engineering* **2018**, *310, 012026.*

[18] Xuan S H, Jiang W Q, Gong X L, et al., Magnetically Separable Fe_3O_4/TiO_2 Hollow Spheres: Fabrication and Photocatalytic Activity, *J. Phys. Chem. C* **2009**, *113, 553-558.*

[19] Feizpoor S, Habibi-Yangjeh A, Ternary TiO_2/Fe_3O_4/$CoWO_4$ nanocomposites: Novel magnetic visible-light-driven photocatalysts with substantially enhanced activity through p-n heterojunction, *J. Colloid Interface Sci.* **2018**, *524, 325-336.*

[20] Liu Z H, Wang G H, Li Y J, et al., Carboxymethyl-β-cyclodextrin functionalized TiO_2@Fe_3O_4@RGO magnetic photocatalyst for efficient photocatalytic degradation of tetracycline under visible light irradiation, *J. Environ. Chem. Eng.* **2024**, *12, 113303.*

[21] Mohapatra J, Xing M, Beatty J, et al., Enhancing the magnetic and inductive heating properties of Fe3O4 nanoparticles via morphology control, *Nanotechnology* **2020**, *31, 275706.*

[22] Wang C, Jiao H, Yang Y B, et al., Dual-Functional S-Scheme Fe_3O_4/TiO_2/g-C_3N_4 double-heterostructure bridged by TiO_2 for collaborative removal of U(VI) and Sb(III), *J. Cleaner Prod.* **2023**, *426, 139114.*

[23] Du C, Mills J P, Yohannes A G, et al., Cascade electrocatalysis via AgCu single-atom alloy and Ag nanoparticles in CO_2 electroreduction toward multicarbon products, *Nat. Commun.* **2023**, *14, 6142.*

[24] Wang C L, Gao W, Liu N Z, et al., Covalent Organic Framework Decorated TiO_2 Nanotube Arrays for Photoelectrochemical Cathodic Protection of Steel, *Corros. Sci.* **2020**, *176, 108920.*

[25] Khan M R, Chuan T W, Yousuf A, et al., Schottky barrier and surface plasmonic resonance phenomena towards the photocatalytic reaction: study of their mechanisms to enhance photocatalytic activity, *Catalysis Science & Technol.* **2015**, *5, 2522-2531*

[26] Zhu C, Yang M Z, Jiang B, et al., Insights into excitonic behavior in single-atom covalent organic frameworks for efficient photo-Fenton-like pollutant degradation, *Nat. Commun.* **2025**, *16, 790.*

[27] Low, Jingxiang, et al. "Heterojunction photocatalysts." *Advanced materials* 29.20 (2017): 1601694.

[28] Tan, Shi Nin, Mei Lian Yuen, and Ros Azlinawati Ramli. "Photocatalysis of dyes: operational parameters, mechanisms, and degradation pathway." *Green Analytical Chemistry* (2025): 100230.

[29] Uheida, Abdusalam, et al. "Visible light photocatalytic degradation of polypropylene microplastics in a continuous water flow system." *Journal of hazardous materials* 406 (2021): 124299.

[30] Jeyaraj, Jeyavani, et al. "Mechanistic vision on polypropylene microplastics degradation by solar radiation using TiO2 nanoparticle as photocatalyst." *Environmental Research* 233 (2023): 116366.

[31] Llorente-García, Brenda Estefanía, et al. "First insights into photocatalytic degradation of HDPE and LDPE microplastics by a mesoporous N–TiO2 coating: effect of size and shape of microplastics." *Coatings* 10.7 (2020): 658.

[32] He, Yanling, et al. "Photocatalytic degradation of different types of microplastics by TiOx/ZnO tetrapod photocatalysts." *Heliyon* 9.11 (2023).

[33] Qin, Jibo, et al. "In-situ formation of Ag2O in metal-organic framework for light-driven upcycling of microplastics coupled with hydrogen production." *Applied Catalysis B: Environmental* 319 (2022): 121940.

[34] Jia, Tingting, et al. "Exploring the photocatalytic degradation mechanism for low-density polyethylene utilizing Bi4Ti3O12 nanoflower catalyst." *Journal of Environmental Chemical Engineering* 12.5 (2024): 113482.

[35] Chai, Chao, et al. "Photocatalytic degradation of polyethylene and polystyrene microplastics by α-

Fe2O3/g-C3N4." *Environmental Science and Pollution Research* 30.58 (2023): 121702-121712.

[36] Khairudin, Khairunnisa, Noor Fitrah Abu Bakar, and Mohamed Syazwan Osman. "Magnetically recyclable flake-like BiOI-Fe3O4 microswimmers for fast and efficient degradation of microplastics." *Journal of Environmental Chemical Engineering* 10.5 (2022): 108275.

[37] Liu, Jiejing, et al. "Enhanced activation of peroxymonosulfate by ZIF-67/g-C3N4 S-scheme photocatalyst under visible light assistance for degradation of polyethylene terephthalate." *Environmental Pollution* 360 (2024): 124682.

[38] Zhou, Dawang, et al. "Feasible degradation of polyethylene terephthalate fiber-based microplastics in alkaline media with Bi2O3@ N-TiO2 Z-scheme photocatalytic system." *Advanced Sustainable Systems* 6.5 (2022): 2100516.

[39] Chen H, Shan X, Qiu X, et al., High-Resolution Mass Spectrometry Combined with Reactive Oxygen Species Reveals Differences in Photoreactivity of Dissolved Organic Matter from Microplastic Sources in Aqueous Environments, *Environmental Science & Technology* **2024**, *58, 10334-10346.*

[40] Wang C L, Liu N Z, Liu X J, et al., Photo-Fenton-like degradation of tetracycline through peroxymonosulfate activation over 2D BiOBr/FeOOH nanosheets and membrane application, *Chem. Eng. J.* **2024**, *491, 151993.*

[41] Zheng N C, Li L J, Tang X H, et al., Spontaneous Formation of Low Valence Copper on Red Phosphorus to Effectively Activate Molecular Oxygen for Advanced Oxidation Process, *Environ Sci Technol* **2023**, *57, 5024-5033.*

[42] Zhu X D, Liu H, Wang J, et al., Investigation of photocatalytic activity of Ag-rutile heterojunctions, *Micro & Nano Letters* **2020**, *15, 1130-1133.*

Commitments on Academic Honesty and Integrity

We hereby declare that we

1. are fully committed to the principle of honesty, integrity and fair play throughout the competition.
2. actually perform the research work ourselves and thus truly understand the content of the work.
3. observe the common standard of academic integrity adopted by most journals and degree theses.
4. have declared all the assistance and contribution we have received from any personnel, agency, institution, etc. for the research work.
5. undertake to avoid getting in touch with assessment panel members in a way that may lead to direct or indirect conflict of interest.
6. undertake to avoid any interaction with assessment panel members that would undermine the neutrality of the panel member and fairness of the assessment process.
7. observe the safety regulations of the laboratory(ies) where we conduct the experiment(s), if applicable.
8. observe all rules and regulations of the competition.
9. agree that the decision of YHSA is final in all matters related to the competition.

We understand and agree that failure to honour the above commitments may lead to disqualification from the competition and/or removal of reward, if applicable; that any unethical deeds, if found, will be disclosed to the school principal of team member(s) and relevant parties if deemed necessary; and that the decision of YHSA is final and no appeal will be accepted.

(Signatures of full team below)

x Qian Wei
Name of team member:

x Meng Zhang
Name of supervising teacher:

Declaration of Academic Integrity

The participating team declares that the paper submitted is comprised of original research and results obtained under the guidance of the instructor. To the team's best knowledge, the paper does not contain research results, published or not, from a person who is not a team member, except for the content listed in the references and the acknowledgment. If there is any misinformation, we are willing to take all the related responsibilities.

Names of team members Qian Wei

Signatures of team members Qian Wei

Name of the instructor Meng Zhang

Signature of the Instructor Meng Zhang

Date

08/21/2025